PHYSICAL REVIEW B VOLUME 35, NUMBER 4 1 FEBRUARY 1987

Interaction of metastable noble-gas atoms with transition-metal surfaces: Resonance ionization and Auger neutralization

W. Sesselmann, B. Woratschek,* J. Küppers, and G. Ertl†
Institut für Physikalische Chemie, Universität München, 8000 München 2, Federal Republic of Germany

H. Haberland
Fakultät für Physik, Universität Freiburg, 7800 Freiburg, Federal Republic of Germany

(Received 2 July 1986)

Electron emission due to deexcitation of metastable noble-gas atoms occurs at transition-metal surfaces which are either clean or covered by atomic adsorbates via resonance ionization of the metastable atom and subsequent Auger neutralization. The resulting electron-energy distributions contain information on the local surface density of states. For analysis, the electron-energy distribution is approximated by a self-convolution function. The validity of this approximation is discussed in detail. The deconvolution of the experimental data yields an effective transition density function reflecting the main features of the electronic surface density of states. The deconvolution technique is described in the Appendix. Furthermore, results are presented on the angular distribution of electrons emitted by Auger neutralization as well as on the lowering of the ionization potential of metastable and ground-state noble-gas atoms at surfaces which provides information on the distance range where resonance ionization, Auger neutralization, and Auger deexcitation occur.

I. INTRODUCTION

Electronically excited metastable noble-gas atoms (X^*) are found to undergo deexcitation with nearly unit probability at solid surfaces.[1] The deexcitation process is based on the interaction of X^* with the electronic states of the outermost surface layer and leads to emission of electrons. Therefore, electron spectroscopy by deexcitation of metastable noble-gas atoms (MDS) is an extremely surface-sensitive method and probes the valence-electronic states of the outermost atomic layer of a solid.[2] It is generally observed that at clean and atomic-adsorbate-covered transition-metal surfaces (with the exception of adsorbed alkali-metal atoms[3]) deexcitation occurs by resonance ionization (RI) followed by Auger neutralization (AN), whereas at surfaces covered with molecular adsorbates frequently Auger deexcitation dominates.[2,4] As shown previously,[5,6] careful evaluation of these AN spectra may provide valuable information on the electronic surface density of states (SDOS). The AN process equally underlies electron emission in ion-neutralization spectroscopy (INS), a technique which had been developed and explored extensively by Hagstrum,[6] and which was the first method yielding information on the valence electronic structures of surfaces. INS uses noble-gas *ions* as primary particles (i.e., the RI process is missing) whose appreciable kinetic energies cause, however, complications[6,7] which are absent with the metastable *neutral* atoms with kinetic energy <0.1 eV applied in MDS. The present work reports on the kind of experimental information which may be obtained by the latter probe, as well as on discussion of the RI and AN processes. Analysis of the AN spectra is based on the theoretical concepts developed originally by Hagstrum,[6] although a phenomenological extension[8] as well as a rigorous quantum-mechanical approach[9] have been published recently. A subsequent paper will deal in detail with data obtained with clean as well as H- and O-covered Pd(111), Cu(110), and W polycrystalline surfaces.[10]

II. EXPERIMENT

The experimental system has been described previously.[4(c)] Metastable noble-gas atoms are generated in a supersonic atomic beam source by electron impact. The beam characteristics of He*, Ne*, and Ar*, respectively, are summarized in Table I. By heating the nozzle source He* atoms with kinetic energies up to 170 meV can be created. Using 120-eV electrons for excitation, more than 90% of the metastable atoms are in the ^1S He*, $^3P_2$ Ne*, and $^3P_2$ Ar* state, respectively.[11] An almost pure ^3S He* beam can be generated by using 30-eV electrons and optically quenching the ^1S He* portion.[11(a)] In Table II the excitation energy E^*, ionization energy E_i, and lifetime of noble-gas atoms in the ground state as well as in the relevant metastable state are listed. The atomic

TABLE I. Mean kinetic energy (E_{kin}), mean velocity (v), and velocity distribution ($\Delta v/v$) for metastable atoms generated in an atomic beam source.

	E_{kin} (meV)	v (m/s)	$\Delta v/v$ (%)
He*	60	1700	11
Ne*	59	750	8
Ar*	71	590	3

TABLE II. Electronic properties of noble-gas atoms in the ground state and in electronically excited metastable states.

	Electronic state	Excitation energy E^* (eV)	Ionization energy E_i (eV)	Lifetime (s)
He	$^1S_0(1s^2)$	0.0	24.580	∞
	$^3S_1(1s\,2s)$	19.820	4.768	4.2×10^3
	$^1S_0(1s\,2s)$	20.616	3.972	2.0×10^{-2}
Ne	$^1S_0(2p^6)$	0.0	21.559	∞
	$^3P_2(2p^5\,3s)$	16.619	4.946	24.4
Ar	$^1S_0(3p^6)$	0.0	15.755	∞
	$^3P_2(3p^5\,4s)$	11.548	4.211	55.9

beam source is connected by a valve to an ultra-high vacuum (UHV) chamber equipped with low-energy electron diffraction (LEED), Auger electron spectroscopy (AES), thermal desorption spectroscopy (TDS), and ultraviolet photoelectron spectroscopy (UPS) facilities. A fully 360°-rotatory electron energy analyzer with about 300-meV energy resolution is used for UPS and MDS measurements. Sample preparation is performed by standard procedures as outlined in Ref. 12 and the cleanness is monitored by LEED, AES, and UPS. Apart from this, the MDS technique itself proves to be most sensitive to the presence of surface impurities.

III. RESONANCE IONIZATION

The nonradiative decay of electronically excited states at metal surfaces may proceed via resonance ionization (RI) and Auger neutralization (AN) or via Auger deexcitation (AD) (Fig. 1). AD results in UPS-like spectra as discussed in Ref. 4. The work function ϕ of transition and noble metal surfaces is generally in the 4—6-eV range, and between the Fermi and vacuum levels a continuous density of unoccupied electronic states exists. Since the ionization energy of metastable noble-gas atoms is in the 4-eV range (Table II), resonance ionization of X^* by tunneling of the excited electron into the unoccupied metal states is highly probable. Electron emission occurs then by subsequent Auger neutralization of the ion X^+ formed at the surface. Typical AN spectra for clean and oxygen-covered Cu(110) surfaces are displayed in Fig. 2 (left-hand side). Compared to the corresponding UP spectra [Fig. 2 (right-hand side)] the maximum kinetic energy of emitted electrons is much lower and the intensity distribution is very different and smooth. Both aspects will be discussed in detail in Sec. IV. AN spectra are observed to be identical for ^1S He* and ^3S He* in spite of the difference of 0.8 eV in excitation energy which is observed in AD spectra.[4] Clearly, the difference in E^* is overcome by RI and the formation of a He$^+$ ion at the surface. RI is the competing process to Auger deexcitation [Fig. 1(a)]. Whether RI or AD dominates depends on the respective transition rates Γ. It is possible for RI to occur if unoccupied (denoted by overbar) electronic states $|\bar{k}\rangle$ at the surface are energetically degenerated with the excited electron state $|a^*\rangle$ of X^*. This means that the local work func-

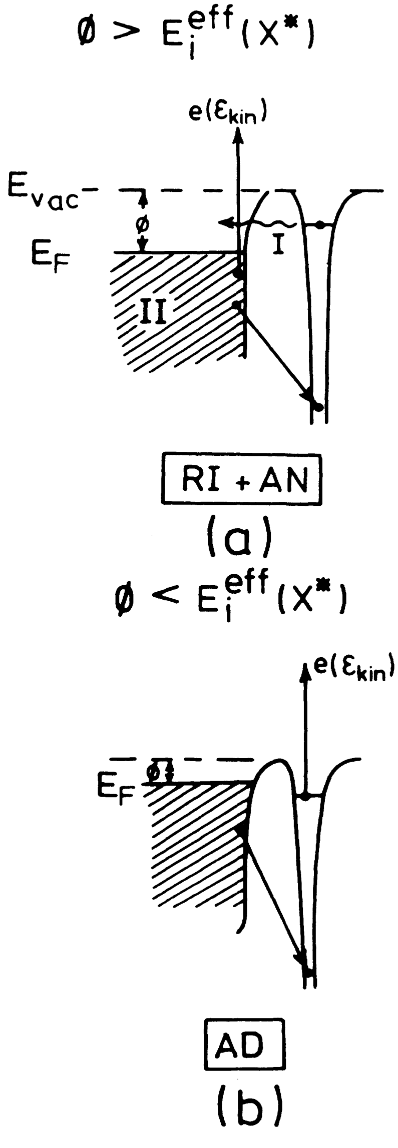

FIG. 1. Deexcitation mechanism of metastable noble-gas atoms (X^*) at surfaces: (a) (I) Resonance ionization (RI) and (II) Auger neutralization (AN), (b) Auger deexcitation (AD). $E_i^{eff}(X^*)$ denotes the ionization energy of X^* at the surface. ε_{kin} is the energy transferred to the emitted electron (e).

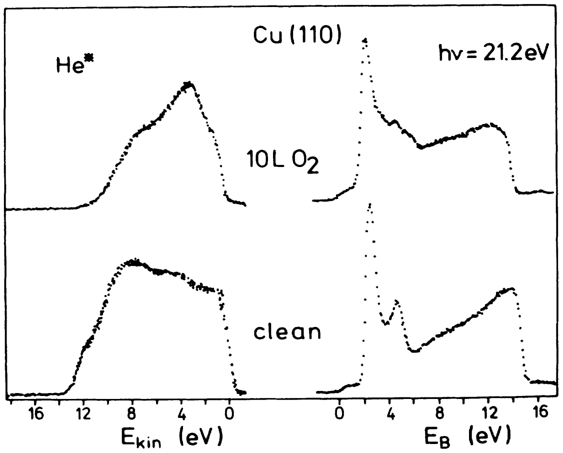

FIG. 2. AN spectra (left) and UP spectra (right) of a clean Cu(110) surface and after exposure to 10 langmuirs O_2 (1 langmuir = 1 L = 10^{-6} Torr s).

tion ϕ_{loc} has to be larger than the ionization energy of X^* at the surface $E_i^{\text{eff}}(X^*)$:

$$\phi_{\text{loc}} > E_i^{\text{eff}}(X^*) \ . \qquad (1)$$

In addition, the respective wave functions must have sufficient overlap for RI to occur. In a first-order approximation Γ_{RI} is determined by the wave-function overlap:

$$\Gamma_{\text{RI}} \sim |\langle a^* | \bar{k} \rangle|^2 \ . \qquad (2)$$

On the other hand, Γ_{AD} will be governed by the overlap of occupied metal states $|k\rangle$ and the core-hole state $|\bar{a}\rangle$ of X^*:

$$\Gamma_{\text{AD}} \sim |\langle k | \bar{a} \rangle|^2 \ . \qquad (3)$$

For clean transition- and noble-metal surfaces relation (1) is fulfilled and it is observed experimentally that RI dominates, i.e., $\Gamma_{\text{RI}} \gg \Gamma_{\text{AD}}$. This is readily understood by simple arguments implied with Eqs. (2) and (3) because the spatial extension of $|a^*\rangle$ is much larger than that of $|\bar{a}\rangle$ and, therefore, the overlap of $|a^*\rangle$ with metal wave functions is more efficient at a given distance from the surface. Calculations for Γ_{RI} yield 10^{-15}–10^{-16} s^{-1}.[13] Experimentally, $\Gamma_{\text{RI}} = 10^{-16}$ s^{-1} has been derived for Ar* and Xe* at metal surfaces.[14] For AD transitions, however, rates in the order of 10^{-13} s^{-1} are quoted.[15] In this context it is interesting to note that for ^1S He* atoms at alkali-metal surfaces an additional competing deexcitation process has been found apart from RI and AD.[3] At these surfaces with very low work function (less than about 3 eV) conversion of ^1S He* to ^3S He* occurs before Auger deexcitation takes place. By arguments similar to those underlying Eqs. (2) and (3) it becomes quite obvious that the transition rate for the conversion process has to be larger than Γ_{AD} as long as conversion is energetically allowed. The transition rate for conversion has been estimated to be about 10^{14} s^{-1}.[16]

In Table III several clean and adsorbate-covered metal surfaces are listed for which we observed experimentally deexcitation of He*, Ne*, and Ar* atoms by the RI + AN process without any indication for the AD process. In some of these cases the work function is smaller than the ionization energy E_i^* of the *free* metastable atom, and one would therefore expect that RI is suppressed and deexcitation occurs via AD. This is not the case. (It should be noted that for surfaces which are either clean or saturated with an adlayer the macroscopic work function ϕ as listed in Table III is equal to ϕ_{loc} as probed by the metastable atoms. This is supported by photoemission studies with adsorbed xenon atoms. These atomic particles probe ϕ_{loc} with about the same spatial resolution.[17]) Therefore, one has to conclude that the *effective* ionization energy $E_i^{\text{eff}}(X^*)$ is reduced in front of a surface. Since the electron configuration of X^* is similar to that of an alkali atom the interaction behavior with surfaces should also be similar. Model calculations[18] for such systems exhibit a

TABLE III. Clean and adsorbate-covered (monolayer saturation coverage) surfaces where deexcitation of metastable noble-gas atoms (X^*) by resonance ionization and Auger neutralization is experimentally observed. ϕ is the work function determined by UPS. (i)–(iv) indicate those systems for which ϕ is smaller than the ionization energy (E_i^*) of the respective metastable atoms [denoted by (i)–(iv)].

Surface	ϕ (eV)	X^*	E_i^* (eV)
Pd(110)	5.2	$^3P_2$ Ne*	4.9 (i)
Pd(111)	5.6	^3S He*	4.8 (ii)
Cu(110)	4.5 (i), (ii)	$^3P_2$ Ar*	4.2 (iii)
W(poly)	4.6 (i), (ii)	^1S He*	4.0 (iv)
Pd(111)/H	5.8		
W(poly)/H	5.2		
Pd(111)/O	6.1		
Cu(110)/O	4.3 (i), (ii)		
W(poly)/O	5.1		
Pd(111)/C_2H_2	4.0 (i), (ii), (iii)		
Pd(111)/C_6H_6	4.0 (i), (ii), (iii)		

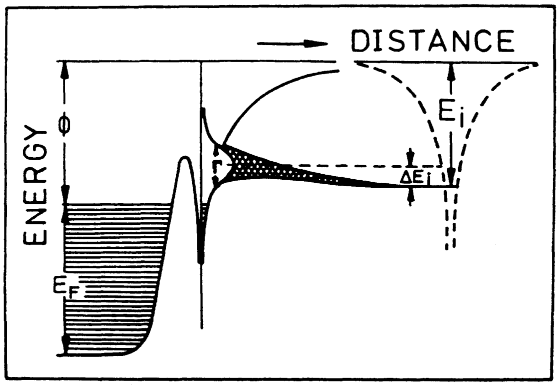

FIG. 3. Energy shift (ΔE_i) and broadening (Γ) of the valence orbital for an atom approaching a metal surface.

significant broadening of the valence state and a reduction of the ionization energy as the atom approaches the metal surface (Fig. 3). Both effects lead to an increasing overlap of unoccupied metal states with the valence states. The half-width of the broadened valence state is directly related to Γ_{RI} and reciprocally to the lifetime of the electron in the atomiclike valence state. Within a distance range of 5—3 Å in front of the surface, valence state half-widths for alkali atoms[18(d)] as well as for Ar* and Xe* atoms[13(e)] have been calculated to be in the order of 0.5—1 eV. The lowering of the ionization energy as the atom approaches the surface is mainly due to the image potential and electron-electron repulsion.[9,18] For Li a lowering of E_i of the order of 0.5—1 eV has been calculated[13(a)] and for Na at a W surface a lowering of E_i of 0.75 eV has been measured.[19]

Thus the experimentally observed dominating RI process for systems where $E_i^* > \phi$ is the consequence of the lowering of E_i^* at surfaces and the broadening of the valence state. Due to the lowering of E_i^* as a function of the distance R between X^* and the surface, RI becomes energetically possible at distances R smaller than R^+ where $E_i^{\text{eff}}(X^*)$ becomes smaller than ϕ_{loc}.[6] R^+ can also be defined as the distance where the initial-state potential curve $V^*(R)$ crosses the final-state ionic curve $V^+(R)$:

$$V^*(R^+) = V^+(R^+) \ . \tag{4}$$

If the R dependence of $V^*(R)$ and $V^+(R)$ would be known, the distance R^+ from which RI becomes energetically possible could be determined. Without attempting a detailed calculation of $V^*(R)$ and $V^+(R)$ Eq. (4) may be approximated by

$$\phi - \frac{c}{(R^+)^6} + S^2 U_{\text{ee}} = E_i^* - \frac{e^2}{4(R^+ - R')} \ . \tag{5}$$

As main effects are considered the electron-electron repulsion S^2U_{ee}, the image-force potential $e^2/4(R^+ - R')$ (Ref. 20), and the van der Waals potential $c/(R^+)$.[6]

U_{ee} is defined as the electron-electron repulsion energy and S denotes the overlap of the wave functions of occupied metal electron states and the excited valence electron of X^*. Reasonable values for U_{ee} and S are 10 eV and 0.1, respectively.[21] This yields for S^2U_{ee} about 0.1 eV. Since this value is close to the uncertainty of the experimentally determined values of ϕ, the term S^2U_{ee} as well as the van der Waals potential which yields values in the meV range are not considered in the following discussion. Thus Eq. (5) may be transformed to

$$R^+ = \frac{e^2}{4(E_i^* - \phi)} + R' \ . \tag{6}$$

R^+ refers to the jellium edge. R' corrects for quantum-mechanical effects concerning the location of the image plane and its value is usually about 0.6 Å.[20,22] Equation (6) may be written as

$$R^+(\text{Å}) = \frac{3.59(\text{eV Å})}{E_i^*(\text{eV}) - \phi(\text{eV})} + 0.6(\text{Å}) \ . \tag{7}$$

In case of adsorbate-covered surfaces (Table III) the value of R' is somewhat uncertain. However, it should not significantly deviate from the value of the clean metal surface. Numerical values for R^+ derived from Eq. (7) for a number of systems where $E_i^* > \phi$ are listed in Table IV. We conclude that for distances smaller than R^+ the RI process will be allowed according to the applied approximation.

Although only a simple model is used to evaluate R^+ and more elaborate theoretical calculations would be desirable, some conclusions can be drawn concerning the deexcitation of X^* atoms at surfaces.

(i) RI dominates over AD also in cases where R^+ is as small as about 5 Å. This shows clearly that up to a distance of about 5 Å Γ_{AD} is still too small for AD transitions to occur although AD is energetically possible in contrast to RI. If, finally, RI becomes energetically allowed at distances less than 5 Å, RI transitions occur with very high probability. This observation shows that AD transitions occur only at distances smaller than about 5 Å.

(ii) A lowering of E_i^* by about 0.9 eV occurs at distances of about 5 Å [see Ne* at Pd(111)/C_2H_2 and Pd(111)/C_6H_6].

Further insight into the distance range of AD transitions is gained from experiments with a potassium surface with $\phi = 2.3$ eV for which no indication of AN emission has been observed by deexcitation of ^3S He*.[3(c)] Equation (7) yields in this case a value of about 2 Å for R^+. Therefore, it can be concluded that at a distance of 2 Å essentially all ^3S He* atoms are deexcited by AD before RI may occur. The relevant distance range for AD transitions of X^* atoms at surfaces is therefore between 2 and 5 Å. In fact, from AD spectra of metastable atoms at alkali-metal surfaces, distances between 3 and 5 Å have been determined where AD transitions occur with maximum probability.[16] RI transitions, on the other hand, can occur with high probability already from distances larger than 5 Å if allowed.

IV. AUGER NEUTRALIZATION

A. Electron energy distribution

If a metastable atom X^* is converted at a solid surface to a positive ion X^+ by resonance ionization (RI), X^+ is

TABLE IV. Calculated R^+ values (in Å). At distances smaller than R^+ resonance ionization is allowed.

Surface	$R^+(^3P_2\ \mathrm{Ne}^*)$	$R^+(^3S\ \mathrm{He}^*)$	$R^+(^3P_2\ \mathrm{Ar}^*)$
Cu(110)	10	13	
W(poly)	13	19	
Cu(110)/O	7	8	
Pd(111)/C_2/H_2	5	5	19
Pd(111)/C_6/H_6	5	5	19

neutralized by a subsequent Auger process [Auger neutralization (AN)] which causes a characteristic energy distribution of emitted electrons known from Hagstrum's ion-neutralization spectroscopy (INS).[6] AN spectroscopy is an extremely surface-sensitive probe[23] because the wave function overlap of the hole state of X^+ with occupied electron states of the solid surface is essential for the AN process. The AN transition involves two electrons originating from electronic states of the solid surface as shown schematically in Fig. 4. The kinetic energy E_{kin} of the emitted electron is given by the energy balance

$$E_{\mathrm{kin}}=E_i^{\mathrm{eff}}-(E+x+\phi_{\mathrm{loc}})-(E-x+\phi)$$
$$=E_i^{\mathrm{eff}}-2E-\phi_{\mathrm{loc}}-\phi\ . \qquad (8)$$

E_i^{eff} describes the effective ionization energy of a (ground-state) noble-gas atom X at the distance R_{AN} in front of the surface where the AN process occurs. E_i^{eff} will be discussed in detail below. E denotes the mean binding energy of the two electrons involved and $2x$ is the respective difference in binding energy. $E_{\mathrm{kin}}=0$ can be easily identified in the spectra by the secondary-electron cutoff. Both the *local* work function ϕ_{loc} and the *macroscopic* work function ϕ come into play because the electron transition to the hole state of X^+ (denoted by H_1 in Fig. 4) is a *local* process at the surface and, therefore, governed by ϕ_{loc}, whereas the emitted electron is detected far outside the surface dipole layer and its kinetic energy is governed by the macroscopic work function ϕ. This has been experimentally shown for a Cu(110) surface covered by a submonolayer of potassium[3(c)] where no energetic shift of the AN emission from bare Cu sites is observed on a $E'_{\mathrm{kin}}=E_{\mathrm{kin}}+\phi$ energy scale [see Eq. (8)] although ϕ decreases about 2 eV. This finding proves that the AN transition is a local probe of the electronic surface structure. If no substantial difference between ϕ and ϕ_{loc} exists (see Sec. III), Eq. (8) may be reduced to

$$E_{\mathrm{kin}}=E_i^{\mathrm{eff}}-2(E+\phi)\ . \qquad (9)$$

According to Eqs. (8) and (9) E_{kin} is independent of x, i.e., pairs of transitions with varying x lead to an identical E_{kin} of the emitted electrons. Following Hagstrum,[6] the energy distribution $P(E)$ of the AN electrons is given by integrating over all combinations of electron transitions:

$$P(E)\sim\int_{-E}^{E}H_1N(E+x)H_2N(E-x)dx\ . \qquad (10)$$

$P(E)$ may be readily converted to $P(E_{\mathrm{kin}})$, the energy distribution of the emitted electrons, by using Eq. (8) or (9), respectively. H_1 and H_2 are the generally energy dependent matrix elements of the Auger transition. $N(E)$ denotes the electronic local density of states at the surface (SDOS).

The AN process has been treated theoretically to various degrees of approximation in a series of papers.[6,8,9,21,24,25] Clearly the matrix elements H_1 and H_2 are complicated functions of energy,[21] in a similar way as with Auger CVV transitions in solids[26] which are related with the processes discussed here. A phenomenological model for approximating the matrix elements was recently proposed by Hood *et al.*[8] which explicitly takes into account the "size" of the orbitals which are involved in the AN process and determine the overlap. If the electronic structure of the outermost atomic layer would be known one could start to compute the matrix elements and from there the AN spectra which then have to be compared with the experimental data. The actual situation is, however, just the opposite: We want to derive information on the SDOS from measured spectra. For this reason we follow in our analysis Hagstrum's "classical" concepts,[24,27,28] whose justification as well as physical interpretation will be discussed in some more detail. It is certainly a good approximation to assume that H_1 depends only on the en-

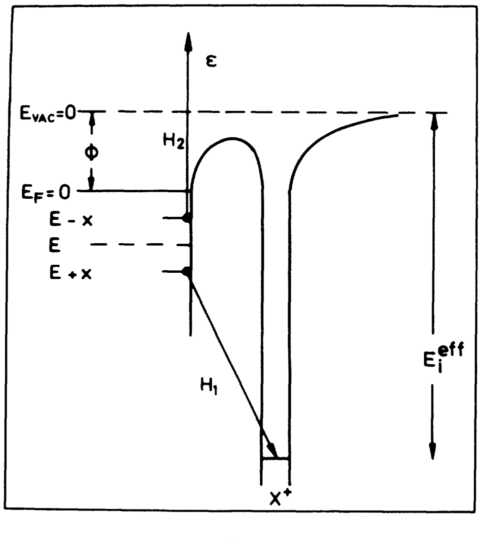

FIG. 4. Energy diagram of the Auger neutralization process (see text). ε denotes the total energy transferred to the emitted electron whereas E_{kin} [see, e.g., Eq. (8)] is the kinetic energy above the vacuum level as experimentally detected. E and E_{kin} are related via $E_{\mathrm{kin}}=\varepsilon-\phi-(E-x)$.

ergy of the initial state: $H_1 = H_1(E+x)$. Therefore the product $H_1 N$ in Eq. (10) can be combined to an "effective transition density" $U_1(E) = H_1(E)N(E)$ representing the SDOS $N(E)$ multipled by H_1. A more severe approximation is probably the assumption that also H_2 depends only on the initial state from which the electron is emitted, yielding $U_2(E) = H_2(E)N(E)$. Equation (10) then reads

$$P(E) \sim \int_{-E}^{E} U_1(E-x)U_2(E+x)dx \ . \tag{11}$$

Without knowledge of $U_1(E)$ or $U_2(E)$ a solution of Eq. (11) is still impossible. However, an *effective* transition density function $U(E)$ as an average of $U_1(E)$ and $U_2(E)$ may be extracted from $P(E)$ by replacing Eq. (11) by a self-convolution function:

$$P(E) \sim \int_{-E}^{E} U(E-x)U(E+x)dx \ . \tag{12}$$

The solution of Eq. (12) is mathematically unique and yields $U(E)$. A procedure to solve Eq. (12) by deconvolution is given in the Appendix. The physical meaning of $U(E)$ has to be discussed carefully. $U(E)$ can be considered as an effective DOS representing the SDOS of the solid surface modified by transition matrix elements which mainly contain the wave-function overlap of electronic SDOS states with the electronic states of the ion at the surface. This latter aspect has been clearly emphasized by Hagstrum and is treated more quantitatively in Ref. 8.

The self-convolution model [Eq. (12)] for $P(E)$ has been also applied for other spectroscopic techniques such as Auger electron spectroscopy[29] and appearance potential spectroscopy[30] where also two valence electrons of the solid are involved and no detailed knowledge on the transition matrix elements exists. For AN spectroscopy the approximation leading to Eq. (11) can be fairly well justified: Experimental AN spectra obtained with various metastable atoms exhibit close similarities.[5,10] He, Ne, and Ar have different ionization energies which means different "excitation energies" [see Eq. (8)]. This indicates that the transition matrix elements predominantly depend on the energy of the initial electronic state. Concerning the certainly more severe self-convolution approximation of Eq. (12) extensive model calculations have been performed by Hagstrum and Becker.[27] The main results may be summarized as follows: In general $U_1(E)$ and $U_2(E)$ contain a smooth background originating from p and s bands of the SDOS and peak structures from localized states and mainly d-band states. Since for $U_1(E)$ and $U_2(E)$ different transition matrix elements play a role, the intensity of the peak structures may be different and in some cases even zero for $U_1(E)$ or $U_2(E)$. Replacing the convolution of $U_1(E)$ and $U_2(E)$ [Eq. (12)] by a self-convolution $U(E) * U(E)$ [Eq. (13)] $U(E)$ shows the following characteristic behavior with respect to $U_1(E)$ and $U_2(E)$.

(i) $U(E)$ is a mean transition density function which contains all peak structures of $U_1(E)$ and $U_2(E)$, respectively. However, the intensity ratio between the background and the peak structures is not reproduced correctly.

(ii) Spurious oscillatory structures may arise in $U(E)$ as a consequence of the deconvolution process. Those spurious structures, however, are easily identified by comparison with the first derivative of $P(E)$, which will be discussed later.

(iii) Additional smooth functions in $P(E)$, such as an electron escape function or additional background, do not alter the characteristics of $U(E)$.

Apparently, $U(E)$ reproduces the essential features of the transition density functions $U_1(E)$ and $U_2(E)$ and thus contains valuable information on the SDOS.

Additional justification for evaluation of AN spectra according to Eq. (12) stems from *CVV* Auger spectroscopy results. Specifically for solid Cu, "atomiclike" *CVV* Auger spectra have been observed and only a small fraction of the spectra can be attributed to a convolution of the Cu d band density of states.[31] The atomiclike *CVV* Auger emission for solid Cu arises because the Coulomb repulsion energy of the two hole states created by the Auger transition in the relatively narrow Cu d band is larger than the double d band width.[32] Therefore, if in case of an AN transition both electrons would originate from Cu d states, a narrow atomiclike $P(E)$ distribution should be observed for the Cu surface which would be distinctly different from that for, e.g., Pd and W surfaces. This is, however, not the case and the experimentally observed $P(E)$ distributions for Cu, Pd, and W are similar in shape.[5,10] These findings indicate that AN transitions do not involve two d electrons but rather predominantly one electron from a sp-like state and one from a d-like state or two sp-type electrons. This appears to be reasonable from the AN process itself because effective wave-function overlap of the hole state of X^+ with sp states will be stronger than that with the more contracted d states. Also theoretical calculations for AN transitions[21] lead to the conclusion that in a convolution approximation for $P(E)$ such as Eq. (11), $U_1(E)$ describes the transition of sp- and d-like states to neutralize X^+ and $U_2(E)$ describes the electron emission occurring mainly from sp-like states. Therefore, the transition density functions $U_1(E)$ and $U_2(E)$ weight the SDOS differently. $U_2(E)$ can be interpreted as the transition density function which reflects the s-like part of the SDOS and should be a smooth function. $U_1(E)$, however, is the transition density function based on the wave-function overlap of the SDOS states with the hole state of X^+ at the surface. Therefore, the intention of using AN spectroscopy is to gain information about $U_1(E)$ which contains the essential features of the SDOS. Since $U_2(E)$ can be expected to be a rather smooth function in a self-convolution approximation, the deconvolution result $U(E)$ reflects the main features of $U_1(E)$.

An alternative approach to the deconvolution procedure of $P(E)$ consists in forming the first derivative of $P(E)$:

$$\frac{dP(E)}{dE} \sim U_1(2E)U_2(0) + U_2(2E)U_1(0) + \int_{-E}^{E} \frac{\delta}{\delta E}[U_1(E-x)U_2(E+x)]dx \ . \tag{13}$$

After reduction of the energy scale by a factor of 2 the first term is proportional to $U_1(E)$. The third term causes oscillatory structures whose intensity depends on the relative peak intensities of $U_1(E)$ and $U_2(E)$.[27] If again $U_2(E)$ is a smooth function compared to $U_1(E)$ the real intensity maxima of $U_1(E)$ are by far more pronounced than those oscillations and $dP(E)/dE$ essentially yields $U_1(E)$.

We used $dP(E)/dE$ to check the validity of the deconvolution result $U(E)$. Formation of the first derivative is usually a more simple procedure than a deconvolution procedure and is often considered to be a more direct approach. Figure 5 shows examples for the deconvolution $U(E)$ as well as the derivative $dP(E)/dE$ of AN spectra from clean and adsorbate-covered Cu and W surfaces. The peak structures which are the most important features of the SDOS are equally present in both sets of data. Also, changes in the relative intensities due to adsorption of oxygen or hydrogen are reflected in the same way by $U(E)$ and $dP(E)/dE$. This holds for the metal d-band region as well as for the emission features at about 5—7 eV below Fermi energy characteristic for adsorbate-induced states. Since $dP(E)/dE$, in contrast to $U(E)$, usually becomes negative, the intensity zero level has been shifted. In general $U(E)$ exhibits a more "conservative" shape because it contains less additional peak structures beside the dominating main features. This is mainly due to the deconvolution algorithm using cubic spline functions (see the Appendix). However, in view of the completely different mathematical procedures the agreement between $U(E)$ and $dP(E)/dE$ is extremely good. In our opinion, this is a very important point to assure the reliability of the analysis of AN spectra and to get valuable information on the SDOS of clean and adsorbate-covered metal surfaces by AN spectroscopy.

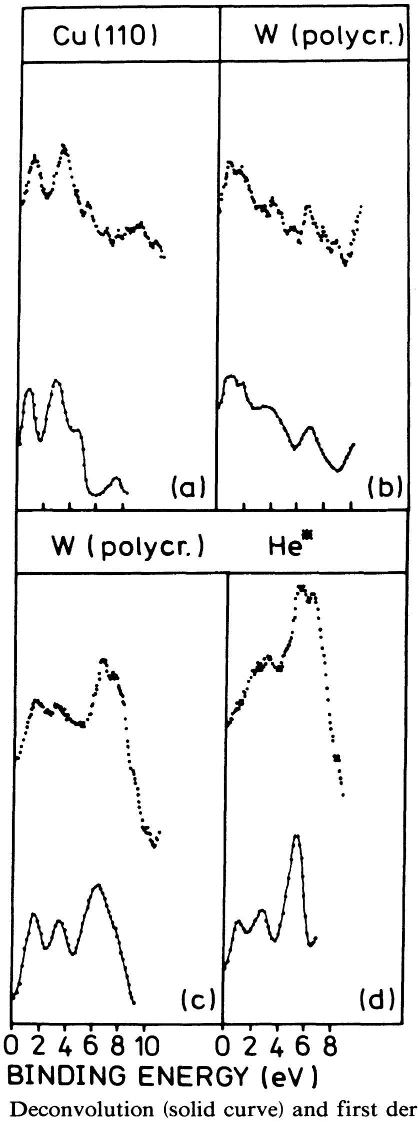

FIG. 5. Deconvolution (solid curve) and first derivative (dotted curve) of Auger neutralization spectra with He* from (a) clean Cu(110), (b) clean W (polycrystalline), (c) W (polycrystalline) exposed to 100 H_2 and (d) W (polycrystalline) exposed to 10 L O_2.

B. Maximum kinetic energy of emitted electrons and the ionization energy of noble-gas atoms at solid surfaces

It becomes evident from Eq. (9) and Fig. 4 that the maximum kinetic energy ($E_{\text{kin,max}}$) of electrons emitted by an AN process is given by

$$E_{\text{kin,max}} = E_i^{\text{eff}} - 2\phi \ . \tag{14}$$

Two electrons from states at the Fermi level ($E=0$) are involved in this AN transition. If the work function ϕ of the surface is known, the ionization energy of the (ground-state) noble-gas atom at the surface (E_i^{eff}) can be determined. Since in ion-neutralization spectroscopy the energy distribution of the emitted electrons is significantly broadened due to the high kinetic energies of the incoming ions[6,7] quantitative information on E_i^{eff} could be obtained only by extrapolating the spectra to zero kinetic en-

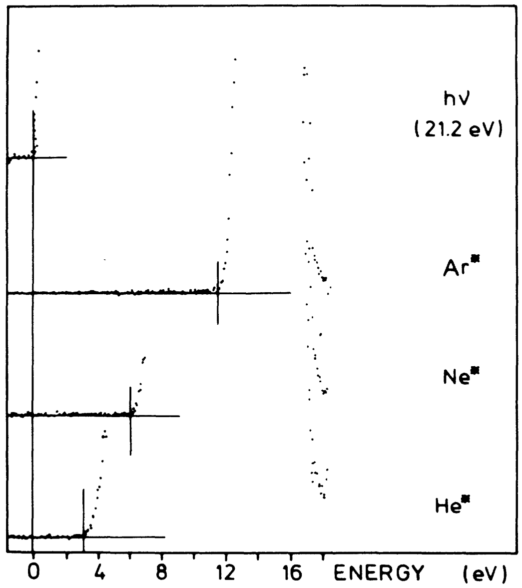

FIG. 6. Emission onset of a 21.2-eV UP spectrum and MD spectra with He*, Ne*, and Ar* from a clean Cu(110) surface.

TABLE V. Experimental values for the ionization energy decrease (ΔE_i) of noble-gas atoms at various surfaces. The work-function change ($\Delta\phi$) due to adsorption at monolayer coverage is also listed.

Surface	$\Delta\phi$ (eV)	ΔE_i (eV) He ($E_i = 24.6$ eV)	Ne ($E_i = 21.6$ eV)	Ar ($E_i = 15.8$ eV)
Pd(111)		2.3	2.3	2.0
Pd(110)		2.0		
Cu(110)		2.1	1.8	1.4
W(poly)		2.2		
Pd(111)/H	0.2	2.3	2.3	2.0
W(poly)/H	0.6	0.6		
Pd(111)/O	0.5	2.1	2.0	2.0
Cu(110)/O	−0.2	2.8	2.3	1.9
W(poly)/O	0.5	1.0		
Pd(111)/C_2H_2	−1.6	0.6		
Pd(111)/C_6H_6	−1.6	1.2	0.9	0.8
Cu(110)/C_2H_2	−0.4	0.7		
Cu(110)/C_6H_6	−0.2	1.4	0.9	0.7

ergy. MDS, however, allows to evaluate E_i^{eff} quite directly. Figure 6 shows the well-defined high kinetic energy onset of electron emission from a Cu(110) surface. He*, Ne*, and Ar* spectra are compared with a 21.2-eV photoelectron (UP) spectrum. E_i^{eff} can be determined independently from the absolute kinetic energy scale by evaluating the energy difference $\Delta E_{\max}$ between the emission onset of the UP spectrum and the X^* spectra, respectively. The difference in maximum kinetic energy of UP (21.2 eV) spectra and AN spectra is given by

$$\Delta E_{\max} = (21.2\ \text{eV} - \phi) - (E_i^{\text{eff}} - 2\phi)\ . \tag{15a}$$

Thus E_i^{eff} can be determined by

$$E_i^{\text{eff}} = 21.2\ \text{eV} - \Delta E_{\max} + \phi\ . \tag{15b}$$

The work function ϕ is determined by the total width of the UP spectrum. In Table V ΔE_i is listed for He, Ne, and Ar atoms at various clean and adsorbate-covered surfaces. ΔE_i is defined as the difference between the ionization energy E_i of the free atom and the ionization energy E_i^{eff} at the surface where the AN transition occurs:

$$\Delta E_i = E_i - E_i^{\text{eff}}\ . \tag{16}$$

ΔE_i is a consequence of the atom-surface interaction. As can be seen from Table V, ΔE_i decreases from He to Ar. Since the ionic radii increase from He^+ to Ar^+ Auger neutralization of Ar^+ should occur at a larger distance from the surface than that of He^+ and the interaction should be weaker and ΔE_i smaller. This effect is more pronounced for the Cu surface than for the Pd surface. Furthermore, ΔE_i depends on the crystallographic surface orientation. On the open Pd(110) surface a lower ΔE_i value is observed than on the close-packed Pd(111) surface. Adsorption of atomic hydrogen and oxygen on Pd and W surfaces causes a decrease in ΔE_i and an increase in $\Delta\phi$, whereas on Cu oxygen adsorption leads to a decrease in $\Delta\phi$ and an increase in ΔE_i. Apparently, $\Delta\phi$ and ΔE_i are related to each other. Adsorption of hydrocarbon molecules leads to a strong reduction of ΔE_i. Probably, these large molecules lead to a larger separation of the noble-gas ions from the metal surface although not sufficient to suppress resonance ionization. So far in the literature quite conflicting ΔE_i values derived from MDS measurements have been reported: For a Ni(111) surface Roussel et al.[4(b)] determined 1.4 eV for He, whereas Bozso et al.[2(c)] report 0.9 eV for He and 0.0 eV for Ne. Our observations are in much better agreement with the findings of Hagstrum who observed at Ni and Cu surfaces ΔE_i values for He of about 2 eV.[6] Careful extrapolation of the INS data to zero kinetic energy yielded at a polycrystalline W surface ΔE_i values of 2.0 eV (He), 2.0 eV (Ne), and 1.8 eV (Ar), respectively.[24,33] From the experimentally observed ΔE_i one can derive the effective ioniza-

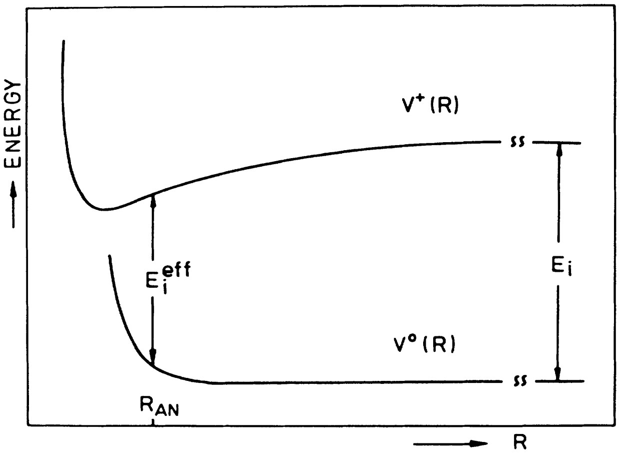

FIG. 7. Potential diagram for Auger neutralization. $V^+(R)$ is the ionic and $V^0(R)$ the neutral potential curve.

tion energy E_i^{eff} of noble-gas atoms in front of the surface at the distance R_{AN} where the Auger neutralization transition occurs. Generally, E_i^{eff} is a function of R, the distance between the atom and the surface. Considering the AN process as an electronic transition between the initial ionic energy curve $V^+(R)$ and the final neutral potential curve $V^0(R)$, $E_i^{\text{eff}}(R)$ is defined as the energy difference between these potential curves (Fig. 7):

$$E_i^{\text{eff}}(R)=V^+(R)-V^0(R) \ . \tag{17}$$

For $R\rightarrow\infty$, $V^+(R)$ and $V^0(R)$ are separated by E_i. Knowledge of $V^+(R)$ and $V^0(R)$ would allow to determine R_{AN} from the experimentally determined E_i^{eff} value. $V^0(R)$ for He atoms at metal surfaces has been calculated by Zaremba and Kohn[34] and by Harris and Liebsch.[35] The maximum potential depth is about 3–8 meV and, therefore, negligible compared to the depth of $V^+(R)$. Thus it is sufficient to approximate $V^0(R)$ by its repulsive part

$$V^0(R)=V^0e^{-aR} \tag{18}$$

with $V^0=12$ eV and $a=2.67$ according to Ref. 35. $V^+(R)$ may be approximated by

$$V^+(R)=E_i+V^+e^{-bR}-\frac{e^2}{4(R-R')}-S^2(R)U_{\text{ee}} \ . \tag{19}$$

The second term represents the repulsive part of $V^+(R)$, the third term is the image potential according to Refs. 20 and 22, and the fourth term takes the electron-electron repulsion into account. R is the distance between the ion and the jellium edge of the metal surface. According to Eqs. (16) and (17), $\Delta E_i(R)$ is given by

$$\Delta E_i(R)=V^0e^{-aR}-V^+e^{-bR}+\frac{e^2}{4(R-R')}+S^2(R)U_{\text{ee}} \ . \tag{20}$$

Reasonable approximations are $U_{\text{ee}}=10$ eV and $S(R)=0.2$ (Ref. 21) because R_{AN} is expected to be certainly smaller than d^+. The smaller radius of the ion compared to that of the neutral is considered by $V^+=0.1V^0$ with $a=b$. $R'=0.6$ Å for Cu.[22] Using these approximations leads to an estimate for R_{AN} of a He^+ ion in front of a Cu surface ($\Delta E_i=2.1$ eV) of about 3 Å. The dominant term in Eq. (20) is the image potential. However, also the electron-electron repulsion potential is of importance. $S(R)=0$ would yield $R_{\text{AN}}=2.5$ Å and $S(R)=0.3$ would give a R_{AN} value of 3.5 Å. Hagstrum and Becker[27] performed similar calculations and determined a R_{AN} value of 2.2 Å from $\Delta E_i=2.0$ eV for a He^+ ion at a W surface. This somewhat lower value results from the use of a classical image potential ($R'=0$), which in this distance range is not appropriate, and from the fact that electron-electron repulsion had been neglected. In any case, the deduced value for R_{AN} can only give some rough guide for the distance where the Auger neutralization transition at surfaces most probably occurs. More elaborate calculations using the experimental ΔE_i values would be necessary to get closer insight into the interaction of noble-gas atoms with surfaces and into the Auger neutralization process.

C. Angular dependence of emitted electrons

Angular-dependent photoemission has been studied quite extensively.[36] Due to wave-vector **k** conservation rules the spectra contain important information on the electronic band structure of solids, as well as on orientation and orbital symmetrics of adsorbates. Since for metastable atoms the deexcitation process is governed by the overlap of localized atomic wave functions with the wave functions of the electronic states at the surface, no such **k** conservation rules come into play. In MDS so far only Auger deexcitation of He* atoms at a CO-covered Pd(110) surface has been investigated in an angular resolved mode.[4(c)] There it had been found that the angular dependence is mainly dominated by the geometrically available impact parameters of the incoming metastable atoms, i.e., by the lateral configuration of the adsorbed molecules. In case of Auger neutralization no theoretical or experimental data were reported so far. Figure 8 shows AN spectra of clean Pd(111) and Cu(110) surfaces, for a fixed angle (45°) of incidence of He* atoms and various electron emission angles. The angular resolution of the electron spectrometer was about 3°. For both surfaces the intensity of electrons emitted from the metal d bands (between 12 and 7 eV kinetic energy) is highest along the surface normal. This holds equally for the s-like states of the Cu(110) surface which are represented in the AN spectra by the shoulder at 12-eV kinetic energy (see Ref. 5). Also for normal incidence of He* atoms the maximum intensity occurs normal to the surface and decreases for larger emission angles. If the emission angle is kept constant and the angle of incidence is varied, emission intensity is maximum at normal incidence and decreases for larger angles of incidence (Fig. 9). The angular dependence is similar for He* and Ne* atoms. The total probability for

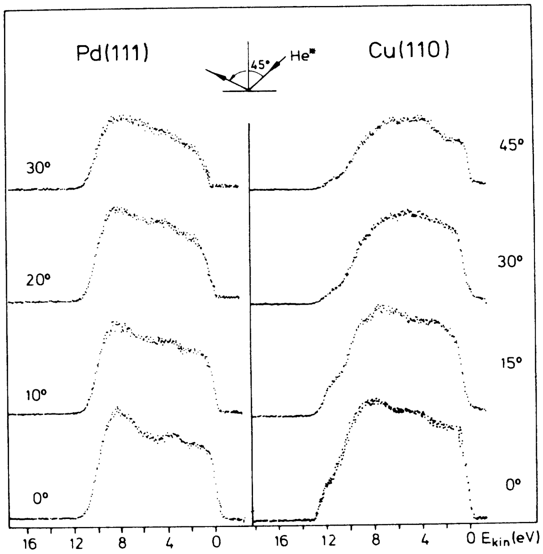

FIG. 8. He* spectra of clean Pd(111) and Cu(110) surfaces at 45° angle of incidence and various electron emission angles.

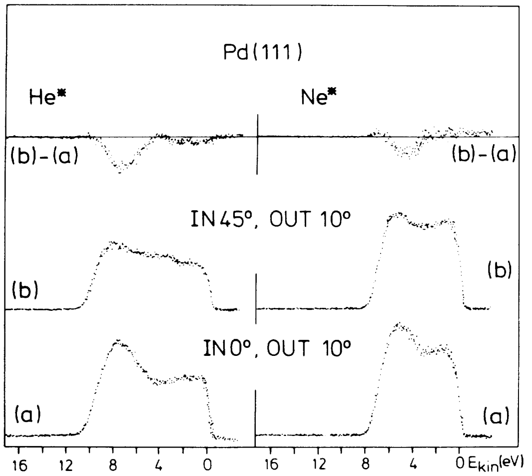

FIG. 9. He* and Ne* spectra of a clean Pd(111) surface at 0° and 45° angle of incidence and an electron emission angle of 10° relative to the surface normal.

deexcitation, on the other hand, was found to be independent of the angle of incidence.[1]

Changing the angle of incidence leads to a variation of the kinetic energy of the He* atoms normal to the surface. However, the higher normal component of kinetic energy for angles close to normal incidence is not responsible for the more intense electron emission. Increasing the kinetic energy of the He* atoms from 60 to 163 meV by heating the nozzle source of the beam caused no noticeable change of the spectra and their angular dependence. Obviously, different kinetic energies up to about 170 meV of the incident metastable atoms do not affect the AN process. In Secs. III and IV B it has been shown that resonance ionization is effective at distances larger than 5 Å from the surface and Auger neutralization occurs at about 3 Å. Over this distance range the ion is accelerated normal to the surface by the image potential. Therefore, the information on the angle of incidence should be lost. The dependence of the electron emission on the angle of incidence appears to be a consequence of the RI process, although the reason for this angle dependence is unclear. For fixed angles of incidence the emission maximum in the direction of the surface normal suggests an anisotropy of the Auger transition. This anisotropy could be partly due to the spatial distribution of the wave functions of the occupied metal states. This has also been suggested in angle-resolved Auger electron spectroscopy studies.[29] Clearly, more experimental and theoretical work would be necessary to obtain a detailed understanding of the angular dependence of the RI and AN process at surfaces.

V. SUMMARY AND CONCLUSIONS

Electron emission due to deexcitation of metastable noble-gas atoms can be used as a sensitive probe for the electronic properties of the outermost atomic layer. At transition-metal surfaces, which are either clean or covered with atomic adsorbates, deexcitation occurs via resonance ionization of the metastable atom and subsequent Auger neutralization. Resonance ionization is allowed if electronic states of the unoccupied surface density of states are energetically degenerated with the excited electron state of the metastable atom. When the metastable atom approaches the surface, the effective ionization energy is lowered and resonance ionization can also occur in cases where the undisturbed ionization energy is too high for RI to be energetically possible. Resonance ionization occurs with very high probability even at distances larger than 5 Å between the surface and the metastable atom. Furthermore, it is shown that the competing Auger deexcitation process operates in a distance range from about 2 to 5 Å. At about 5 Å the ionization energy is decreased by about 0.9 eV. Auger neutralization involves two electrons from the surface valence levels. The resulting electron distribution contains information on the local surface density of states (SDOS). For analysis of these Auger neutralization spectra the electron energy distribution is approximated by a self-convolution function as proposed by Hagstrum.[6] These approximations are discussed in detail. The deconvolution of the experimental spectra leads to an effective transition density function which reflects the essential features of the local surface density of states. The results of our deconvolution procedure are also compared with the first derivative of the Auger neutralization spectra. In the Appendix the deconvolution technique is discussed, and in a forthcoming paper detailed results will be presented.[10] The maximum kinetic energy of electrons emitted due to the Auger neutralization process allows to determine the effective ionization energy of noble-gas atoms at a distance of about 3 Å from solid surfaces. Depending on the specific surface and the type of noble-gas atoms, the ionization energy is lowered by about 0.5 to 2.5 eV. The angular dependence of Auger neutralization electron emission exhibits maximum intensity normal to the surface. As a function of the angle of incidence maximum intensity is observed at normal incidence. It is found that the normal component of the kinetic energy of the incident metastable atoms is not decisive for the observed angular dependence.

ACKNOWLEDGMENT

Financial support of this work by the Deutsche Forschungsgemeinschaft (Sonderforschungsbereich SFB 128) is gratefully acknowledged.

APPENDIX

Deconvolution of Auger neutralization spectra

In Sec. IV A the analysis of Auger neutralization spectra has been reduced to the solution of a self-convolution integral. Equation (12) is identical with the self-convolution function $S(y)$:

$$S(y)=\int_{-y}^{y} f(y-x)f(y+x)dx \ . \tag{A1}$$

$f(y)$ is the expected deconvolution result and represents $U(E)$ in Eq. (12). The deconvolution of experimental AN spectra poses two major problems: the mathematical task to find the solution $f(y)$ from a given database of $S(y)$ values, and the limitations due to the experimental uncertainties of measured values $\widetilde{S}(y)$. The solution $f(y)$ of Eq. (A1) is mathematically unequivocal except of the sign.[37] To calculate $f(y)$ from $S(y)$ several methods have been developed which are based on a step-by-step deconvolution technique,[27] on discrete Fourier transformation,[38] or on the use of interpolating spline functions.[37,39] In a mathematical sense all these procedures are equivalent. Differences, however, come into play in dealing with experimentally determined values $\widetilde{S}(y)$. With the first method[27] uncertainties accumulate very easily, while with the second method[38] the phase problem is very serious.[38(c)] Interpolating spline functions used in Refs. 37 and 39, however, allow very easily to account for the limited accuracy of measured data $\widetilde{S}(y)$.[40] The algorithms proposed in Refs. 37 and 39 are very similar. In the present work the mathematical formalism presented in Ref. 37 is applied because it is very direct and simple.

Algorithm

$S(y)$ is given at $k+1$ equally spaced points y_i. $f(y)$ can be composed of spline functions of the order q defined in the k subdivided intervals. Then, $f(y)$ is a polynomial of the order $2q-1$:

$$f(y)=\sum_{j=1}^{q} b_j y^{j-1}+\sum_{i=1}^{k} b_{q+i}\frac{(y-y_i)_+^{2q-1}}{(2q-1)!}\ , \tag{A2}$$

with

$$(y-y_i)_+=\begin{cases}0 & \text{for } y\le y_i\ ,\\ y-y_i & \text{for } y>y_i\ .\end{cases}$$

b_1-b_{q+k} are adjustable parameters. Inserting Eq. (A2) in Eq. (A1) yields

$$\begin{aligned}S(y)=&\sum_{j=1}^{q}\sum_{m=1}^{q} b_j b_m\frac{(j-1)!(m-1)!}{(j+m-1)!}y^{j+m-1}\\&+2\sum_{j=1}^{q}\sum_{h=1}^{k} b_j b_{q+h}\frac{(j-1)!}{(2q+j-1)!}(y-y_h)_+^{j+2q-1}\\&+\sum_{i=1}^{k}\sum_{h=1}^{k} b_{q+i}b_{q+h}\frac{(y-y_h-y_i)_+^{4q-1}}{(4q-1)!}\ .\end{aligned} \tag{A3}$$

The measured data $\widetilde{S}(y)$ (AN spectrum) are digitized into a set of M values $\widetilde{S}(y_j)$ equally spaced on the energy scale. Now the function

$$F(b_1,\ldots,b_{q+k})=\sum_{j=1}^{M}|\widetilde{S}(y_j)-S(y_j)|^2 \tag{A4}$$

is minimized by using a Levenberg-Marquardt algorithm.[41] This yields the optimum set of parameters b_1-b_{q+k} for approximation of the experimental data by $S(y)$. The knowledge of b_1-b_{q+k} gives immediately the deconvolution solution $f(y)$.

The space d between two points y_i in $S(y)$ or $f(y)$ on the interval of M data points is given by

$$d=M/k+q+1\ . \tag{A5}$$

Empirically it has been found that $q=2$ provides sufficient flexibility for the interpolating spline functions. M and d should be chosen appropriately so that $k+q$ does not exceed the value of 20, because then the Levenberg-Marquardt algorithm converges very slowly or even does not reach the absolute minimum of $F(b_1,\ldots,b_{q+k})$. Figure 10 shows two examples of a deconvolution of the self-convolution of a model density-of-states function $f(y)$ consisting of two Lorentzians and a linearly increasing background.

Deconvolution (c) covers more data points ($M=96$) and, therefore, d has to be chosen larger than for deconvolution (d). The smaller d in Fig. 10(d) gives a better resolution in the deconvoluted spectrum but only a smaller part of the spectrum can be deconvoluted. The experimental spectra have been deconvoluted with $M=60$ and $d=4$. This provides sufficient resolution, deconvolution of nearly the complete experimental spectrum, and still fast convergence of the Levenberg-Marquardt algorithm. The typical calculation time on a Cyber 170 was 100—200 s.

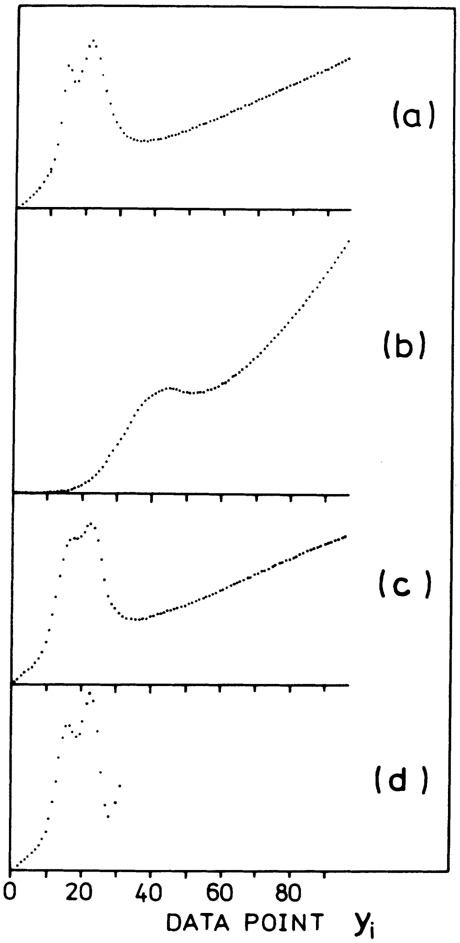

FIG. 10. (a) Model density of states, (b) self-convolution, (c) deconvolution with $M=96$, $d=8$, and $q=2$, and (d) deconvolution with $M=32$, $d=4$ and $q=2$.

Influence of the limited accuracy of experimental data

The limited accuracy of the experimental data $\tilde{S}(y_j)$ due to noise and statistics has to be considered very carefully because this is the real problem in deconvolution of Auger neutralization spectra. Experimental data must not directly be treated by an algorithm based on an exact mathematical function. Either the algorithm has to be modified, so that the spline functions do not interpolate but just approximate the experimental data or the data have to be smoothed to define a quasi-mathematical-function. The first procedure has been implemented in the deconvolution algorithm by Dose *et al.*[39(b)] In the present work the data have been smoothed by use of a fast-Fourier-transform algorithm because then the data which really enter the deconvolution procedure can always be directly compared with the original data as well as with the back-convolution of the deconvoluted result. Because of the limited accuracy of the experimental data the deconvolution is no longer unequivocal. Therefore, the deconvolution result has to satisfy several conditions.

(i) The approximation of $S(y_j)$ to the smoothed data $\tilde{S}(y_j)$ has to be as good as possible (convergence criterion).

(ii) The smoothest positive function $f(y_j)$ has to be chosen as solution.

(iii) The validity of the deconvolution result has to be checked by comparison with the first derivative of the AN spectrum (see Sec. IV A).

These conditions are based on necessary physical and numerical requirements. To look for the smoothest solution $f(y_j)$ is partly guaranteed by the use of spline functions. This may sometimes obscure "real peals" in the deconvolution result but leads to reliable results. Several deconvolutions of an experimental spectrum are also necessary to identify the onset $[\tilde{S}(O)]$ of the experimental spectrum which may be obscured by noise.[27] Figure 11 shows the minimum value R of $F(b_1, \ldots, b_{q+k})$ for various $\tilde{S}(O)$ points. The best values R are found within four experimental data points. The range of convergence is very well defined because the R values outside are orders of magnitude larger. On the energy scale of the experimental spectrum four data points correspond to 600 meV, just twice the experimental resolution of the electron energy analyzer. Therefore, the conditions (i)—(iii) and the search for the minimum R guarantee that the absolute minimum of $F(b_1, \ldots, b_{q+k})$ is reached. It should be noted that the same experimental spectra have also been deconvoluted with the algorithm of Dose *et al.*[39(b)] and very good agreement of the results has been found. Certainly, deconvolution of experimental spectra which represent a self-convolution function has to be done very carefully, but reliable and meaningful results can be obtained if an appropriate algorithm is used and reasonable convergence criteria are imposed and satisfied.

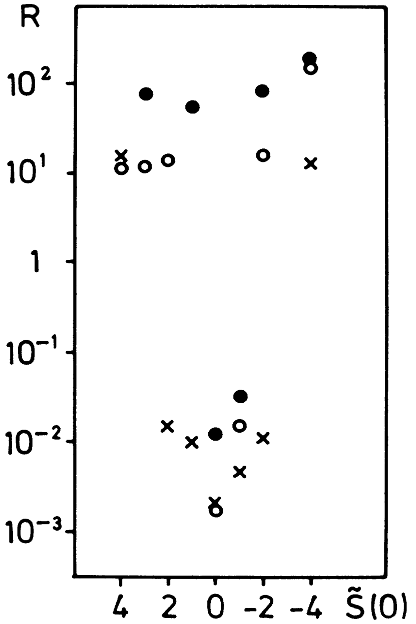

FIG. 11. Convergence factor R for various $\tilde{S}(O)$ data points which define the onset of the experimental spectrum. The different symbols represent different experimental spectra.

---

*Present address: IBM Almaden Research Center, San Jose, CA 95120-6099.

†Present address: Fritz-Haber-Institut der Max-Planck-Gesellschaft, 1 Berlin 33, Federal Republic of Germany.

[1] H. Conrad, G. Doyen, G. Ertl, J. Küppers, W. Sesselmann, and H. Haberland, Chem. Phys. Lett. **88**, 281 (1982); H. Conrad, G. Ertl, J. Küppers, W. Sesselmann, B. Woratschek, and H. Haberland, Surf. Sci. **117**, 98 (1982).

[2] (a) H. Conrad, G. Ertl, J. Küppers, S. W. Wang, K. Gerard, and H. Haberland, Phys. Rev. Lett. **42**, 1082 (1979); (b) F. Mucchielli, C. Boiziau, R. Nuvolone, and J. Roussel, J. Phys. C **13**, 2441 (1980); (c) F. Bozso, J. T. Yates, Jr., J. Arias, H. Metiu, and R. M. Martin, J. Chem. Phys. **78**, 4256 (1983).

[3] (a) J. Lee, C. Hanrahan, J. Arias, F. Bozso, R. M. Martin, and H. Metiu, Phys. Rev. Lett. **54**, 1440 (1985); (b) B. Woratschek, W. Sesselmann, J. Küppers, G. Ertl, and H. Haberland, *ibid.* **55**, 611 (1985); (c) B. Woratschek, W. Sesselmann, J. Küppers, G. Ertl, and H. Haberland, *ibid.* **55**, 1231 (1985).

[4] (a) H. Conrad, G. Ertl, J. Küppers, W. Sesselmann, and H. Haberland, Surf. Sci. **100**, L461 (1980); (b) J. Roussel, C. Boiziau, R. Nuvolone, and C. Reynard, *ibid.* **110**, L634 (1981); (c) H. Conrad, G. Ertl, J. Küppers, W. Sesselmann, and H. Haberland, *ibid.* **121**, 161 (1982); (d) F. Bozso, J. Arias, C. Hanrahan, R. M. Martin, J. T. Yates, Jr., and H. Metiu, *ibid.* **136**, 257 (1984); (e) W. Sesselmann, B. Woratschek, G. Ertl, J. Küppers, and H. Haberland, *ibid.* **146**, 17 (1984).

[5] W. Sesselmann, H. Conrad, G. Ertl, J. Küppers, B. Woratschek, and H. Haberland, Phys. Rev. Lett. **50**, 446 (1983).

[6] H. D. Hagstrum, in *Electron and Ion Spectroscopy of Solids*, edited by L. Fiermans, J. Vennik, and W. Dekeyser (Plenum, New York, 1978), and references therein.

[7] C. A. Moyer and K. Orvek, Surf. Sci. **114**, 295 (1982); **121**, 138 (1982); C. A. Moyer, K. W. Brown, and H. F. Helbig, *ibid.*

143, 591 (1984).

[8]E. Hood, F. Bozso, and H. Metiu, Surf. Sci. **161**, 491 (1985).

[9]F. von Trentini and G. Doyen, Surf. Sci. **162**, 971 (1985).

[10]W. Sesselmann, B. Woratschek, J. Küppers, G. Ertl, and H. Haberland (unpublished).

[11](a) B. Brutschy and H. Haberland, Phys. Rev. A **19**, 2232 (1979); (b) T. Munakata, K. Kuchitsu, and Y. Harada, Chem. Phys. Lett. **64**, 409 (1979); J. Electron Spectrosc. Relat. Phenom. **20**, 235 (1980).

[12]R. G. Musket, W. McLean, C. A. Colmenares, D. M. Makowiecki, and W. J. Siekhaus, Appl. Surf. Sci. **10**, 143 (1982).

[13](a) M. Remy, J. Chem. Phys. **53**, 2487 (1970); (b) R. K. Janev, J. Phys. B **7**, 1506 (1974); (c) R. K. Janev and N. N. Nedeljkovic, *ibid.* **14**, 2995 (1981); (d) T. B. Grimley, V. C. Jyothi Bhasu, and K. L. Sebastian, Surf. Sci. **124**, 305 (1983); (e) N. D. Lang, A. R. Williams, F. J. Himpsel, B. Reihl, and D. E. Eastman, Phys. Rev. B **26**, 1728 (1982).

[14]Ph. Avouris, J. E. Demuth, and N. J. DiNardo, J. Phys. (Paris) Colloq. **44**, 451 (1983).

[15]H. Haberland, Y. T. Lee, and P. E. Siska, Adv. Chem. Phys. **45**, 487 (1981).

[16]B. Woratschek, W. Sesselmann, J. Küppers, G. Ertl, and H. Haberland, Surf. Sci. (to be published).

[17]K. Wandelt, J. Vac. Sci. Technol. A **2**, 802 (1984).

[18](a) J. W. Gadzuk, Surf. Sci. **6**, 133, 159 (1967); Phys. Rev. B **1**, 2110 (1970); (b) J. W. Gadzuk, J. K. Hartmann, and T. N. Rhodin, *ibid.* **4**, 24 (1971); (c) N. D. Lang and W. Kohn, *ibid.* **1**, 4555 (1970); **3**, 1215 (1971); (d) J. P. Muscat and D. M. Newns, Surf. Sci. **74**, 355 (1978); **84**, 262 (1979).

[19]E. G. Overbosch, B. Rasser, A. D. Tenner, and J. Loss, Surf. Sci. **92**, 310 (1980).

[20]J. A. Appelbaum and D. R. Hamann, Phys. Rev. B **6**, 1122 (1972).

[21]F. v. Trentini, Ph.D. thesis, University of Munich, 1985 (unpublished).

[22]J. Schmit and A. A. Lucas, Solid State Commun. **11**, 419 (1972).

[23](a) V. Heine, Phys. Rev. **151**, 561 (1966); (b) J. A. Appelbaum and D. R. Hamann, Phys. Rev. B **12**, 5590 (1975); (c) J. C. Tully, *ibid.* **16**, 4324 (1977).

[24]H. D. Hagstrum, Phys. Rev. **96**, 336 (1954).

[25](a) M. L. E. Oliphant and P. B. Moon, Proc. R. Soc. London, Ser. A **127**, 338 (1930); (b) H. S. W. Massey, Proc. Cambridge Philos. Soc. **26**, 386 (1930); **27**, 469 (1931); (c) S. S. Shekhter, Sov. Phys.—JETP **7**, 750 (1937); (d) A. Cobas and W. E. Lamb, Jr., Phys. Rev. **65**, 327 (1944); (e) C. A. Moyer and K. Orvek, Surf. Sci. **114**, 295 (1982).

[26](a) P. J. Feibelman and E. J. McGuire, Phys. Rev. B **17**, 690 (1978); P. J. Feibelman, E. J. McGuire, and K. C. Pandey, *ibid.* **15**, 2202 (1977); (b) D. R. Jennison, *ibid.* **18**, 6865 (1978); D. R. Jennison, H. H. Madden, and D. M. Zehner, *ibid.* **21**, 430 (1980); (c) J. D. Dow and C. P. Flynn, J. Phys. C **13**, 1341 (1980); J. N. Schulman and J. D. Dow, Phys. Rev. Lett. **47**, 371 (1981).

[27]H. D. Hagstrum and G. E. Becker, Phys. Rev. B **4**, 4187 (1971).

[28]H. D. Hagstrum, Phys. Rev. **150**, 495 (1966); **159**, 572 (1967).

[29]R. Weissmann and K. Müller, Surf. Sci. Rep. **1**, 251 (1981).

[30]R. L. Park and J. E. Houston, J. Vac. Sci. Technol. **10**, 176 (1973); **11**, 1 (1974).

[31](a) C. J. Powell, Solid State Commun. **26**, 557 (1978); (b) H. H. Madden, D. M. Zehner, and J. R. Noonan, Phys. Rev. B **17**, 3074 (1978); (c) R. Weissmann and K. Müller, Surf. Sci. Rep. **1**, 251 (1981).

[32](a) M. Cini, Solid State Commun. **20**, 655 (1976); **24**, 681 (1977); (b) G. A. Sawatzky, Phys. Rev. Lett. **39**, 504 (1977); (c) M. Cini and A. D'Andrea, Phys. Rev. B **29**, 6540 (1984).

[33]H. D. Hagstrum, Phys. Rev. **104**, 317 (1956).

[34]E. Zaremba and W. Kohn, Phys. Rev. B **15**, 1769 (1977).

[35]J. Harris and A. Liebsch, Phys. Rev. Lett. **49**, 341 (1982).

[36]E. W. Plummer and W. Eberhardt, Adv. Chem. Phys. **49**, 533 (1982).

[37](a) C. Garot and C. Boiziau, Le Vide **96**, 17 (1979); (b) C. Boiziau, C. Garot, R. Nuvolone, and J. Roussel, Surf. Sci. **91**, 313 (1980).

[38](a) W. M. Mularie and W. T. Peria, Surf. Sci. **26**, 125 (1971); (b) J. A. Tagle, V. Martinez Saez, J. M. Rojo, and M. Salmeron, *ibid.* **79**, 77 (1978); (c) V. Martinez Saez, J. Electron Spectrosc. Relat. Phenom. **17**, 33 (1979); (d) P. Szabo and G. J. Roussel, *ibid.* **33**, 115 (1984).

[39](a) J. H. Onsgaard and P. Morgan, J. Vac. Sci. Technol. **15**, 44 (1978); (b) V. Dose, Th. Fauster, and H.-J. Gossmann, J. Comput. Phys. **41**, 34 (1981); V. Dose and H. Scheidt, Appl. Phys. **19**, 19 (1979).

[40]I. J. Schoenberg, Q. Appl. Math. **4**, 45 (1946).

[41](a) D. W. Marquardt, J. Soc. Ind. Appl. Math. **11**, 431 (1963); (b) K. M. Brown and J. E. Dennis, Numer. Math. **18**, 289 (1972).